NUMERICAL ASPECTS OF THE PREDICTION OF THE FAR FIELD RADIATION FROM FLAMES USING AN INTEGRAL METHOD

Rafael Piscoya*[1], Haike Brick[1], Martin Ochmann[1], Peter Költzsch[2]

[1]TFH Berlin -University of Applied Sciences
13353 Berlin, Germany
piscoya@tfh-berlin.de

[2]Technical University Dresden,
01062 Dresden, Germany

ABSTRACT

Turbulent flames can produce noise with high pressure levels. If the flames are open, the sound waves result from the direct combustion noise which involves the generation of local hot regions (hot spots). The sound is produced by a sudden volume expansion of the hot gas due to the combustion process. If the flames are enclosed, for example by a combustion chamber, the reflected waves affect the direct noise but can also induce oscillations of the chamber walls. These oscillations radiate sound to the exterior. The corresponding waves together with the sound waves that emerge through the openings of the chamber (for example: the exhaust) contribute to the total radiated sound of the enclosed flame.

This paper studies the use of an integral method to determine the far field radiation of open and enclosed flames with special attention to the numerical aspects of the technique presented.

1 INTRODUCTION

The acoustic far field produced by turbulent flames cannot be determined currently using only a Computational Fluid Dynamics (CFD) simulation because the computational cost would be enormous. Instead, hybrid methods, in which the turbulent reactive flow in the source region and the acoustic far field are computed separately, are more effective and require less computational time and resources. Since two very different methods have to be coupled, an important task in this hybrid approach is to perform an appropriate matching of both methods.

For the computation of the far field, we use a method based on the Helmholtz Integral Equation (HIE) which involves only evaluation of surface integrals. Thus, the discretization of the three-dimensional space required for the calculation of volume integrals or the direct solution of the wave equation is avoided.

In the present work, the numerical aspects of the coupling of the CFD code with the acoustic method are described for the case of an open flame and the necessary processing of the data provided by the CFD is shown.

2 INTEGRAL APPROACH

The acoustic pressure p produced by the flame in the far field can be determined using an integral method. To perform the calculation, the flame is enclosed by a surface S, which is typically referred as *Kirchhoff* surface or as *control* surface. At this surface S, at least one of two acoustic quantities (p, $\partial p/\partial n$) or a combination of both has to be known. To ensure the validity of the integral method, two assumptions are made:

a) All acoustic sources are located inside S ,

b) Outside S, the medium is homogeneous, at rest and the Helmholtz equation holds (see Fig. 1).

$$\nabla^2 p + k_0^2 p = 0 \qquad (1)$$

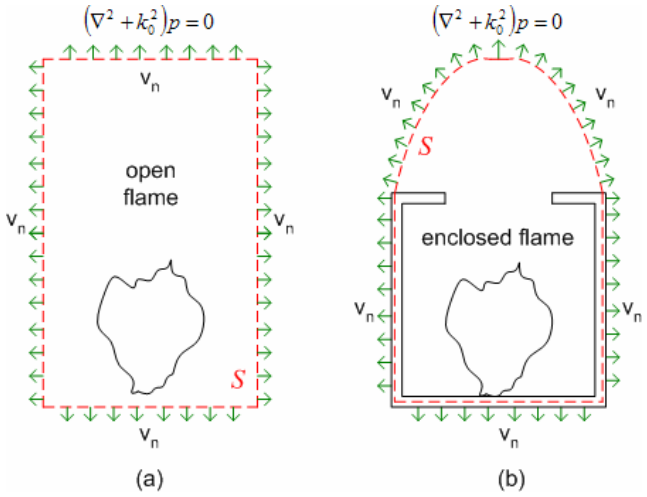

Figure 1: Flame model for the calculation of the far field a) open flame; b) enclosed flame

The sound pressure at any point outside or on *S* is given by the expression [1]:

$$C(\vec{x})\,p(\vec{x}) = \int_S \left(p(\vec{y})\frac{\partial g(\vec{x},\vec{y})}{\partial n(\vec{y})} - \frac{\partial p(\vec{y})}{\partial n(\vec{y})} g(\vec{x},\vec{y}) \right) dS(\vec{y}), \quad (2)$$

which is the known as the Helmholtz integral equation (HIE) with *C* given by

$$C(\vec{x}) = \begin{cases} 0 & \vec{x} \text{ inside } S \\ 0.5 & \vec{x} \text{ on } S \\ 1 & \vec{x} \text{ outside } S \end{cases}. \quad (3.a)$$

g is the Green's function in the free field

$$g(\vec{x},\vec{y}) = \frac{\exp(-jk|\vec{x}-\vec{y}|)}{4\pi|\vec{x}-\vec{y}|}, \quad (3.b)$$

$k=\omega/c$ is the wavenumber, ω the angular frequency and c the speed of sound in the acoustic domain outside *S*. The time dependence $\exp(j\omega t)$ is omitted.

In a medium at rest, pressure *p* and particle velocity $\vec{v}$ are related by the equation

$$\vec{v} = \frac{j}{\omega\rho}\nabla p, \quad (4)$$

hence in Eq. (1), $\partial p/\partial n$ can be replaced by $-j\omega\rho v_n$.

$$C(\vec{x})\,p(\vec{x}) = \int_S \left(p(\vec{y})\frac{\partial g(\vec{x},\vec{y})}{\partial n(\vec{y})} + j\omega\rho v_n(\vec{y}) g(\vec{x},\vec{y}) \right) dS(\vec{y}) \quad (5)$$

According to Eq. (5), in case sound pressure and particle velocity are known at the control surface, the determination of the sound pressure at any point outside *S* is simply a surface integration over *S*.

If only one acoustic quantity, *p* or v_n, is prescribed at the surface, the integral equation in Eq. (5) can be rearranged in a system of equations after a discretization of *S*

$$H\hat{p} - G\hat{v}_n = 0, \quad (6)$$

where *H* and *G* are the system matrices and $\hat{p}$ and $\hat{v}_n$ the variable vectors. The solution of this system of equations will be the unknown acoustic variable at *S*. Once both acoustic variables are known on *S*, Eq. (5) can be numerically evaluated for every $\vec{x}$ outside *S*. This procedure is usually referred to as the Boundary Element Method (BEM).

3 COUPLING VARIABLES

For the open flame (see previous works [2]-[5]), the values of the velocity field at a set of cylindrical control surfaces enclosing a turbulent open diffusion flame were extracted from a LES calculation performed at the Technical University Darmstadt. In that simulation, the values of the pressure at the surfaces could not be provided by the LES and had to be first computed following Eq. (5).

The incompressible LES code does not couple density and pressure. Density fluctuations, which are considerably high in the combustion zone, are nevertheless considered. For the low Mach numbers of the flow, this approximation allows saving computational costs and gives a satisfactory representation not only of the flow mean quantities, but also of the chemical characteristics. The fluid dynamic properties of the numerical results agree very well with experimental data [6].

4 DATA PROCESSING

The CFD and the BEM are very different approaches. They work in different domains, time/frequency, with different time/frequency and spatial resolutions. Thus a direct transfer of the data from one method to the other is not possible. A processing of the CFD data must be performed before they can be used by the acoustic method. In the following subsections, a review of the operations and transforms carried out on the data are presented.

4.1 Generation of the acoustic mesh

The LES mesh is much finer than it is necessary for the acoustic requirements. Additionally, for acoustical purposes, a non-uniform surface mesh leads to an increase of computational costs without an increase of accuracy. Therefore the LES grids were coarsened in axial and radial directions until the resolution met the tangential resolution and the assembling of uniform quadratic surface elements was possible. Fig. 2 illustrates this mesh generation.

Ten concentric cylindrical surface meshes with increasing radii were built, so that acoustical simulations on the basis of different enveloping surfaces were possible. The frequency limit for the validity of the model can be obtained considering the six-elements-per-wavelength rule, which bases primarily on the Shannon sampling theorem [7].

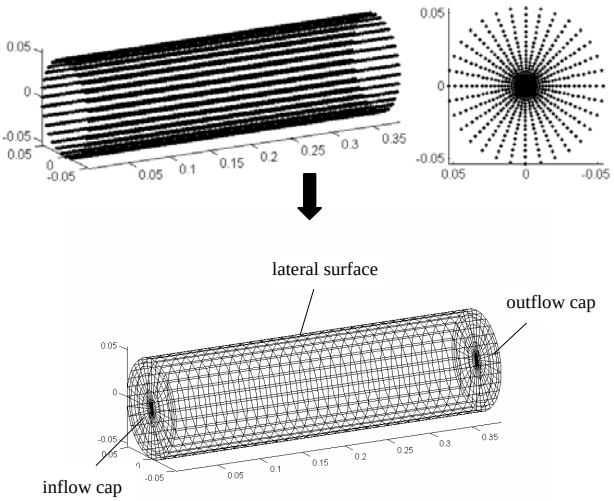

Figure 2: Generation of an equidistant acoustical surface mesh (below) from the grid points of the LES (above)

4.1.1 The downsampling

This mesh coarsening comes along with a downsampling of the given LES-Data. The influence of the downsampling process was investigated and the results are presented in the following. The mesh was coarsened in axial and radial direction. The velocity data at the coarsened grid nodes can be sampled pointwise out of the finer mesh (in case the grid nodes of both meshes coincide) or can be sampled in conjunction with a convolution with a spatial filter. The simplest filter is a rectangle filter, which results in the so called simple moving average. We applied both, the pointwise and filtered sampling. A major or minor aliasing effect for the pointwise sampling is expected depending on the smoothness of the original normal velocity curve [8, Ch. 4]. The filtering with a the rectangle window function along the coarsened grid coordinates represents a low-pass filtering of the original signal and provides a minimization of the aliasing effect. The aliasing effect occurs in the wavenumber spectrum. The wavenumber spectrum $V(k_n)$ results from the Fourier transform from the spatial to the wavenumber domain, which is defined as

$$V(k_n) = \frac{1}{l}\int_0^l v(x)e^{jk_n x}dx\,.$$

Fig. 3 shows the normal velocity in axial direction at the first node line of lateral surface of the tenth cylinder of the original and coarsened mesh.

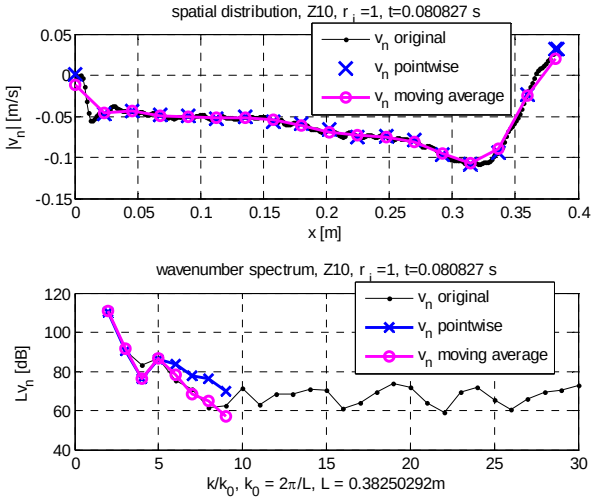

Figure 3: Instantaneous velocity distribution in axial direction *x* at t = 0.081s for axial line 1, *upper panel:* spatial distribution, *lower panel:* wavenumber spectrum

It can been seen, that the velocity distribution is quite smooth, the pointwise extracted data extraction as well as the filtered data (moving average) follow well the curve of the given data. Nevertheless, in the wavenumber spectrum an aliasing effect can be observed in the higher wavenumber range for the pointwise sampling. Please note, that the wavenumber spectrum of the coarsened mesh is limited to 10 k/k_0 due to cruder sampling.

Fig. 4 shows the velocity and its spectrum for the same line at a later time step. The spatial velocity distribution appears again to be smooth enough to be well represented by the pointwise extraction as well as by the averaged data. Here, we find a wavenumber spectrum, which does not show an aliasing effect for both of the sampling methods.

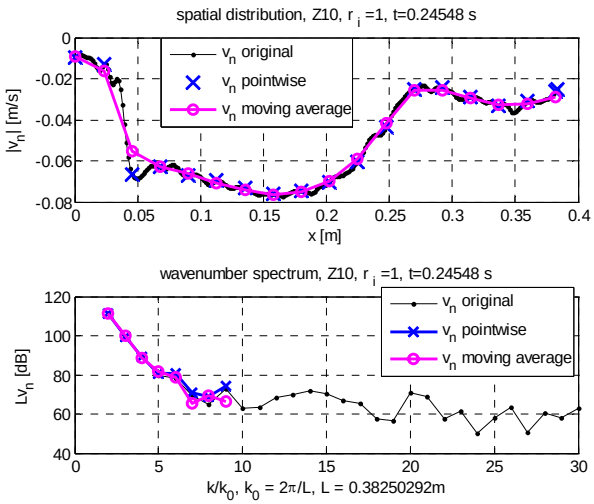

Figure 4: Instantaneous velocity distribution in axial direction *x* at t = 0.245s for axial line 1, *upper panel:* spatial distribution, *lower panel:* wavenumber spectrum

Fig. 5 shows exemplarily the normal velocity distribution at the outflow cap along the first radial line. Here, the averaging smoothes the original curve, which shows some short wave fluctuations. A direct transform in the wavenumber domain is not possible for the velocity distribution in radial direction, since the mesh is not equidistant in this direction.

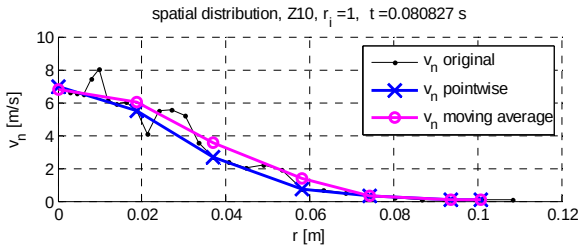

Figure 5: Instantaneous velocity distribution in radial direction *r* at t = 0.081s for radial line 1

From the wavenumber spectra shown for line 1 for different time steps we see, that a resulting aliasing effect from a pointwise sampling depends strongly on the velocity curve of the originally given data. The pointwise extraction does not necessarily lead to an aliasing effect, but the moving average is the more secure sampling method.

What effect will result from an aliasing effect in the wavenumber domain? An increase of the wavenumber spectra as seen in Fig. 3 can lead to a higher sound radiation level in the higher and middle frequency range. In generally, the smaller the wavelength of a wave on the Kirchhoff-surface, the more sound waves will be produced in the higher frequency range. That means vice versa that the aliasing shift of higher spectral components to lower spectral components could result in a wrongly increased sound radiation mainly in the middle and higher frequency range. But one has to keep in mind, that Fig. 3 and 4 show only instantaneous velocity distributions, the curves change with every time step and for every axial node line.

In Fig. 6 the radiated sound power of the tenth control surface for a pointwise data sampling and a filtered sampling is presented. Unlike as assumed, the sound power does not differ significantly for both sampling methods.

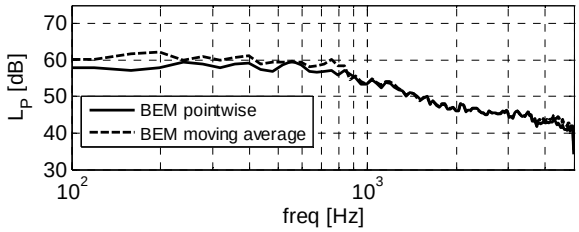

Figure 6: Radiated sound power level L_p of the tenth control surface for a pointwise and filtered data sampling

As discussed in a previous article [9] the outflow cap was detected to determine mainly the amount of radiated sound power. In a next step we do not coarsen the mesh in radial direction at the outflow cap, but include all available data in the grid generation of the surface mesh and subsequently in the velocity data sampling. Hence, the velocity distribution

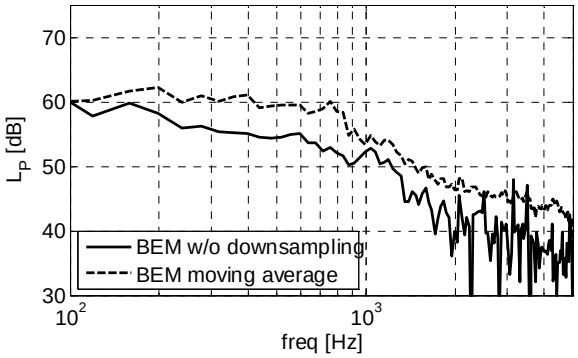

Figure 7: Radiated sound power level L_p of the tenth control surface for a complete data sampling at the outflow cap and filtered data sampling on the coarsened mesh.

on the outflow cap has the same fine resolution as the LES Data. It was shown in Fig. 5 labeled as "v_n original". In axial direction the grid is still coarsened as before. Fig. 7 shows the resulting sound power level for the filtered sampling and for the case of no downsampling on the outflow cap.

In this case a more significant effect can be observed. The radiated sound power is overestimated by using the coarsened mesh over the whole frequency range, though the data were sampled via moving averaging.

A closer look at the radiated sound from the outflow cap reveals the strong influence of the coarsening. Fig. 8 shows the sound power, which is radiated only from the outflow cap's surface and this is considerably increased by the mesh coarsening.

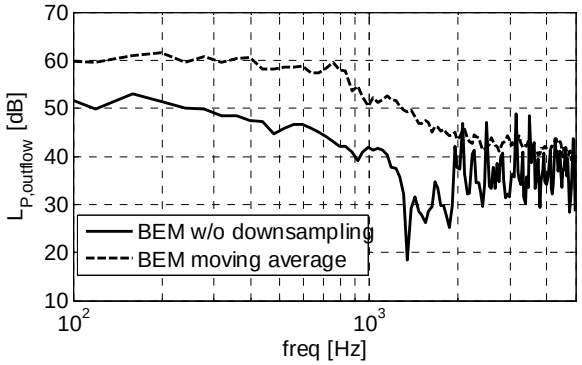

Figure 8: Radiated sound power level L_p from the outflow cap of the tenth control surface for a complete data sampling at the outflow cap and filtered data sampling on the coarsened mesh.

The resulting radiated sound depends strongly on the used mesh. It seems that the data sampling on the coarsened mesh with a simple moving average filtering is not able to reproduce the velocity distribution adequately. Other authors also report remarkable differences of their CAA-solutions depending of the use of fine or coarse grids [10].

To use simply the original LES-grid is not a solution for this problem, since the essential idea of all hybrid methods of various CFD-CAA coupling strategies is to use grids, which are adequate for the particular methods. The large difference in the characteristic fluid mechanical and acoustic length scales require a finer time and spatial resolution for the fluid simulation as for the acoustic simulation. With the use of the coarsened grid for the acoustic simulation the sound radiation of the flame can be determined at reasonable computational time and effort. Further research work should be devoted to more elaborated filtering techniques.

4.2 Location of the control surface

The location of the control surface is a very sensible point of this coupling strategy. Eq. (5) is valid only if the control surface is placed in a region where the medium is uniform and at rest. This situation represents the most favourable case, since the sound field is then completely given by the surface integral. When the source region is large and the control surface cannot be placed in the homogeneous region, Eq. (5) will produce an error.

A way for testing if the control surface is placed in a homogeneous medium is by comparison of the sound power. The sound power is obtained integrating the sound intensity over a closed surface. In n homogeneous medium, the sound power is independent of the dimension and location of the surface if it encloses all sound sources. Thus, by calculating the sound power using different surfaces, we expect to determine which surfaces are placed fully in the homogeneous medium.

This idea was applied to the open flame case. Ten cylindrical control surfaces having the same length but different radii were used to compute the sound power (Fig. 9).

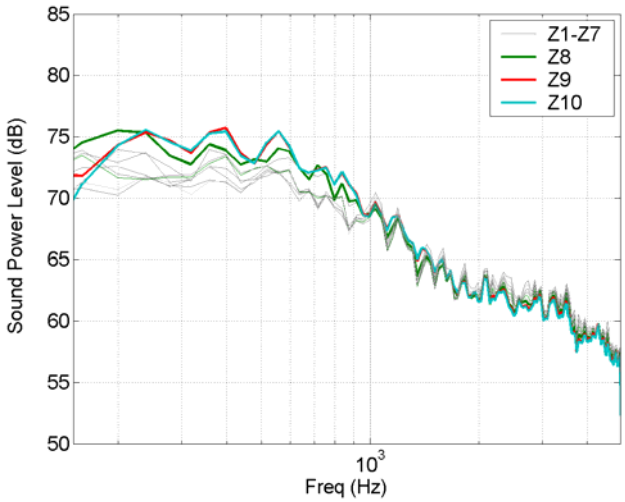

Figure 9: Sound power curves calculated with each of the ten cylinders

In Fig. 9, the curves of the sound power are compared. It can be seen that the curves are practically identical above 1000 Hz. Below that frequency, there are differences but a certain convergence could be found for the last two cylinders (Z9 and Z10). According to the above results, the last cylinder, which has the biggest radius, was considered for the computation of the sound radiation.

4.3 Inclusion of ground effects

In practical situations, the flames are located in a certain environment (room, laboratory, etc). Assuming that side walls and ceilings have some type of acoustical treatment, the scenario will be more similar to a half space problem than to a free field problem. The presence of the ground can be directly included in Eq. (5) by using an appropriate Green's function $g(\vec{x},\vec{y})$.

The Green's function in the presence of an infinite plane has a simple expression only in two ideal cases, when the acoustic impedance Z: a) is infinite ($Z\to\infty$) and b) is zero (Z=0). The first case corresponds two a rigid plane and the second to a soft plane.

The expression for the Green's function is given by:

$$g(\vec{x},\vec{y}) = \frac{e^{-jkR_1}}{4\pi R_1} + R\frac{e^{-jkR_2}}{4\pi R_2} \qquad (7)$$

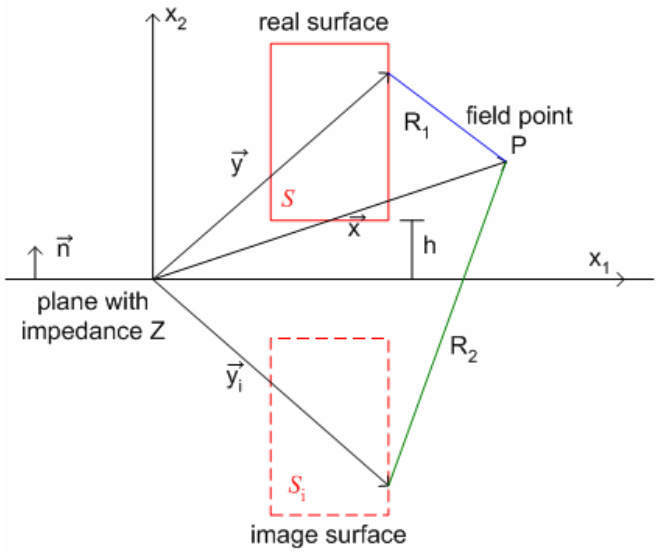

Figure 10: Sketch of real and image surface in the presence of a reflecting plane

with $R_1 = |\vec{x} - \vec{y}|$, $R_2 = |\vec{x} - \vec{y}_i|$ and R having a value +1 if the plane is rigid and -1 if the plane if soft. The vector $\vec{y}$ defines a point over the real surface and the vector $\vec{y}_i$ defines the position of its image point with respect to the plane (see Fig. 10).

A calculation of the sound field of the open flame with and without the two types of planes was performed. In Figs. 11 and 12, the radiation patterns and the curves of sound power of the flame for the three cases: free space, rigid plane and soft plane are shown. In the plots of the radiation patterns (Fig. 11), the superposition of direct and reflected waves cause a local increase and decrease of the sound pressure compared to the free space case. The radiated sound power is sensitive to the presence of the planes only in the lower frequency range (Fig. 12). The presence of a soft or rigid plane leads to a slight decrease or increase of the sound power level in this frequency range, respectively. Generically, the influence of these types of planes on the radiated sound power decrease with the distance h of the flame from the plane. In case $kh >> 1$, where k is the wavenumber, the influence of an ideal rigid or soft plane on the radiated sound power can be almost neglected.

Nevertheless, the directivity of the sound field is strongly affected by the presence of a plane, independently of h, and has to be considered when doing sound power measurements. In the higher frequency range, only a careful scanning of the intensity or of the sound pressure on an enveloping surface around the flame can give reliable results due to the mentioned effects.

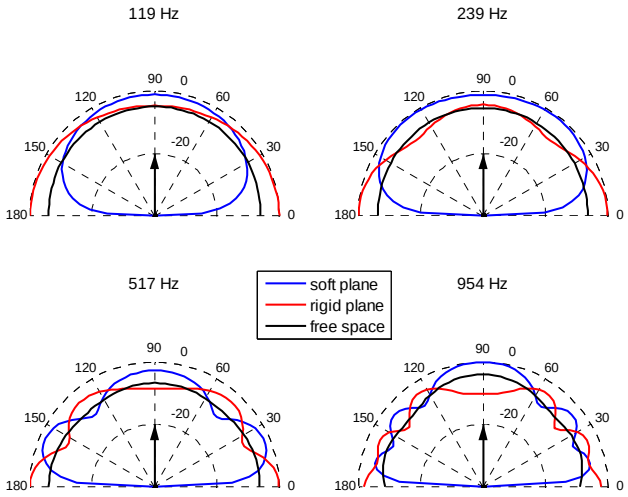

Figure 11: Comparison of radiation patterns of the normalized sound pressure level. The arrow indicates the direction of the flow. The flames control surface is located on a soft plane, on a rigid plane or in free space, respectively.

The presented simple image source ansatz is not suited to describe the sound propagation above an impedance plane with finite and complex impedance, which show damping and spring/mass characteristics. An appropriate Greens function, which is able to describe the sound propagation above an impedance plane and is in addition suitable for an implementation into a BEM code, is thoroughly discussed in [11] and [12]. It is planned to apply this new formulation also to the investigated flames.

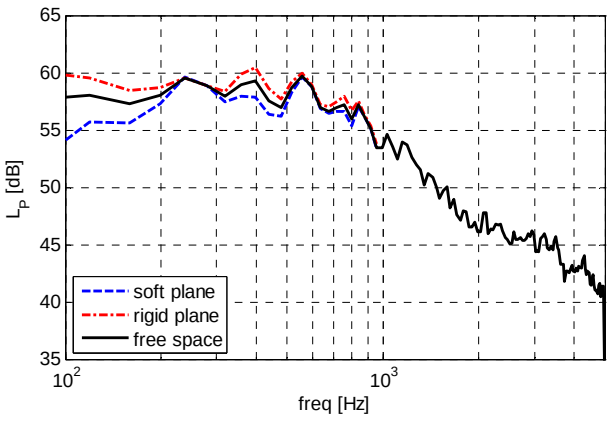

Figure 12: Comparison of sound power spectra. The control surface is located above on a soft plane, on a rigid plane and in free space, respectively.

4.4 Determination of the velocity spectra with reduction of the variance

The integral approach described in section 2 provides a method to determine the acoustic field of the flame in the frequency domain. Since the LES works in the time domain, the LES data have to be first transformed from the time to the frequency domain applying a Fourier Transform.

The original time steps of the LES are in the range of 10^{-7}s. For the acoustic calculation a data sampling of 10^{-4} s was chosen to establish a frequency range of [0-5000] Hz, which should cover the spectral radiation of the flames. Hence, the instantaneous data were directly written out without any low pass-filtering.

Since only one time series was provided and the power spectrum of the whole signal involves a high variance, the time series were split into sets of 250 samples, so that each set was used as input velocity for one sound field calculation. The predicted sound power and sound pressure level in the far field are the average over all these individual calculations.

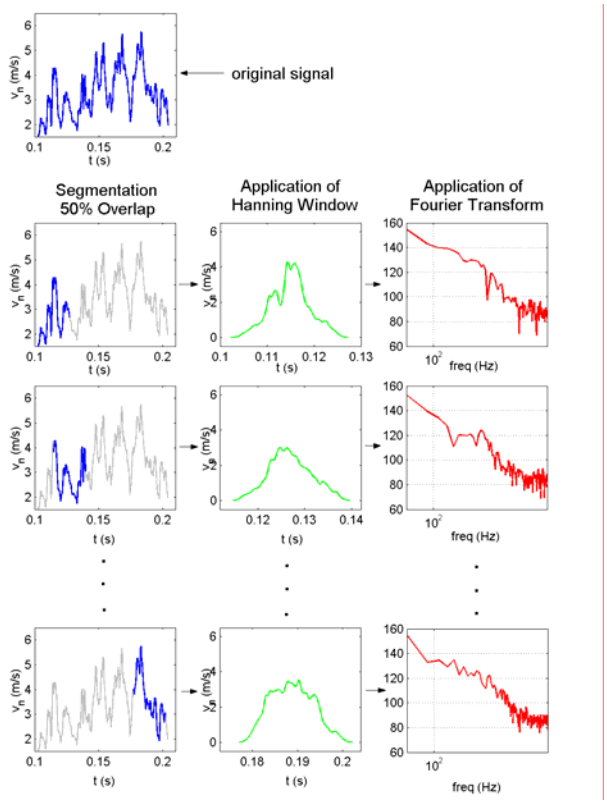

Figure 13: Scheme of the computation of the velocity spectra

In order to increase the number of individual sets and therefore decrease the variance of the averaged spectrum, an overlap between adjacent segments was considered. According to Welch [13], a 50% overlap along with the use of a Hanning window reduce the aliasing effects as well as keep the dependence between segments in a low level. In Fig. 13, the procedure to compute the velocity spectra is shown. As a result of the segmentation, the frequency resolution is decreased. Since each segment had 250 time samples and the time step was 10^{-4} s, the frequency resolution was 40 Hz.

5 COMPARISON WITH MEASUREMENTS

The sound power of the investigated flame was experimentally determined. The jet burner was located in a facility without acoustic treatment, for this reason intensity measurements were preferred over pressure measurements to determine the sound power. The radiation patterns were not measured since free field conditions were not fulfilled. The jet flames were thin and long so that the temperature did not represent a problem at all. Only at the top of the flame, a few centimeters away from the flame axis, the sound intensity could not be measured.

The measurements were made when all activities in the laboratory had finished and all other equipments were switched off in order to avoid the presence of disturbing sound sources. A measurement of the background noise was made and it was well below the flame noise above 100 Hz. A first test measurement confirmed the axial symmetry of the sound. Thus, the number of measured points was reduced to 28. A more detailed description of the measurement setup can be found in [9].

The sound radiation of the diffusion flames was calculated using the velocity at the surfaces of the cylinder enclosing the flame. For each velocity spectrum (see section 4.4) a radiated sound field is computed and the resulting sound field is obtained by averaging all calculations:

$$P_{avg}(f) = \frac{1}{N}\sum_{i=1}^{N} P_i(f) \qquad (8)$$

The shape of the simulated curves of the open flame in Fig. 14 agrees well at frequencies below 1 kHz but the amplitude is about 3 dB overestimated. Above 1 kHz, the slope of the decay differs a little from the measured decay.

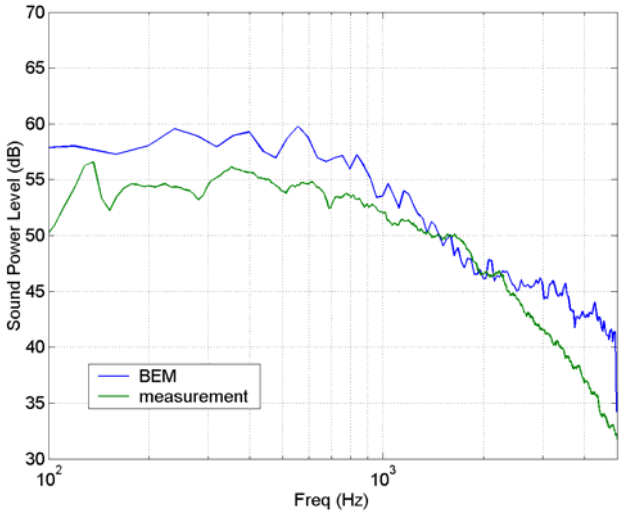

Figure 14: Simulated and measured sound power level of the open flame

6 SOUND PROPAGATION IN A NON-HOMOGENEOUS MEDIUM

If the medium outside the control surface enclosing the flame is non homogeneous, Eq. (1) is not valid. In case the non homogeneous region outside the chamber can be described as a source distribution q, an inhomogeneous Helmholtz equation can be derived:

$$\nabla^2 p + k_0^2 p = q \quad , \tag{9}$$

and its integral form gives this expression for the sound pressure [14]:

$$C(\bar{x})p(\bar{x}) = \int_S \left(p(\bar{y}) \frac{\partial g(\bar{x},\bar{y})}{\partial n(\bar{y})} - \frac{\partial p(\bar{y})}{\partial n(\bar{y})} g(\bar{x},\bar{y}) \right) dS(\bar{y}) - \int_V q(\bar{y}) g(\bar{x},\bar{y}) dV(\bar{y}) \tag{10}$$

Comparing Eqs. (10) and (2), we see there is an additional volume integral over the source term q.

For the case of flames burning in the free (half)space, it is reasonable to think that the non homogeneous region does not extend over the whole space but is limited to a volume Ω as depicted in Fig. 15. Outside Ω, the Helmholtz equation (1) does hold.

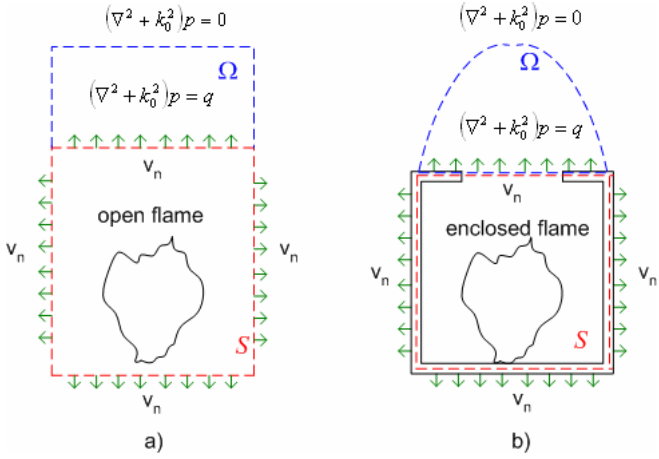

Figure 15: Flame model including a non homogeneous region Ω for a) open flame; b) enclosed flame

To find the sound field at all positions outside S, we proceed dividing the outer space in two regions. Region I corresponds to the volume Ω and region II to the homogeneous region.

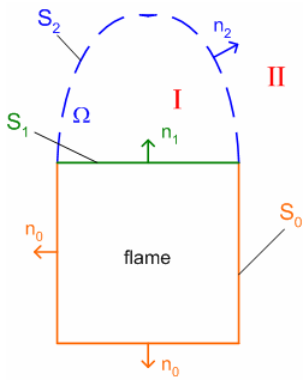

Figure 16: Surfaces and domains for the sound field determination

We subdivide S into two surfaces: S_0 and S_1. S_1 is the common surface between the volume enclosed by S and Ω. S_0 is then $S \setminus S_1$. Volume Ω is enclosed by $S_1 \cup S_2$ (see Fig. 16). We have to solve a set of two differential equations, one in each region

$$\begin{aligned} \left(\nabla^2 + k_0^2\right) p_I &= q \quad \text{in Region I} \\ \left(\nabla^2 + k_0^2\right) p_{II} &= 0 \quad \text{in Region II} \end{aligned} \tag{11}$$

and also have to satisfy the following boundary conditions:

$$\begin{aligned} v_n &= v_S \quad \text{on } S_0 \cup S_1 \\ p_I &= p_{II} \quad \text{on } S_2 \\ v_{nI} &= v_{nII} \quad \text{on } S_2 \end{aligned} \tag{12}$$

The integral forms of Eqs. (11) give us two sets of equations,

$$\begin{aligned} C_I p_I &= \int_{S_1 \cup S_2} \left(p_I^S \frac{\partial g}{\partial n} - \frac{\partial p_I^S}{\partial n} g \right) dS - \int_\Omega q g_1 dV \\ C_{II} p_{II} &= \int_{S_0 \cup S_2} \left(p_{II}^S \frac{\partial g}{\partial n} - \frac{\partial p_{II}^S}{\partial n} g \right) dS \end{aligned} \tag{13}$$

with two constants C_I and C_{II} whose values are "complementary":

$$C_I = \begin{cases} 1 & \text{in } \Omega \\ 0.5 & \text{on } S_1 \cup S_2 \\ 0 & \text{outside } \Omega \end{cases}, \quad C_{II} = \begin{cases} 0 & \text{in } \Omega \\ 0.5 & \text{on } S_0 \cup S_2 \\ 1 & \text{outside } \Omega \end{cases}$$

The integral equation for region I contains a volume integral which leads to high computational cost, since it has to be completely evaluated for every field point. To avoid performing this volume integral, we introduce the "Dual Reciprocity" approach. This method allows us to replace the volume integral with a sum of surface integrals.

This is obtained by first expanding the source distribution in a series of functions f_j:

$$q(\vec{x}) = \sum_j \alpha_j f_j(\vec{x}) \tag{14}$$

The basic idea of the method consists in finding some functions ψ_j that are solutions of an inhomogeneous Helmholtz equation with function f_j as source term:

$$\left(\nabla^2 + k_0^2\right)\psi_j = f_j \tag{15}$$

The integral form of Eq. (15) gives an expression for the volume integral over $f_j g$ in terms of ψ_j:

$$-\int_\Omega f_j g dV = C_I \psi_j + \int_{S_1 \cup S_2} \left(\psi_j^S \frac{\partial g}{\partial n} - \frac{\partial \psi_j^S}{\partial n} g \right) dS . \tag{16}$$

By substituting Eqs. (16) and (14) into the first equation in (13), the final equation for p_I depending only on surface integrals is obtained:

$$\begin{aligned} C_I p_I = &\int_{S_1 \cup S_2} \left(p_I^S \frac{\partial g}{\partial n} - \frac{\partial p_I^S}{\partial n} g \right) dS \\ &+ \sum_j \alpha_j \left(C_I \psi_j + \int_{S_1 \cup S_2} \left(\psi_j \frac{\partial g}{\partial n} - \frac{\partial \psi_j}{\partial n} g \right) dS \right) \end{aligned} \tag{17}$$

We can obtain a system of equations similar to Eq. (6) by discretizing surfaces S_0, S_1 and S_2. In Eq. (17) the coefficients α_j must be determined. Assuming the source distribution q is known at a set of N points at the surface $S_1 \cup S_2$ and at L points in the volume Ω, and considering $M=L+N$ terms of the sum in Eq. (14), M α_j's can be computed.

This technique was tested using a "spherical flame" with different source distributions. The source terms were chosen dependent only on the distance to the center of the sphere because in that case, analytical solutions can be found for certain source functions. The numerical solutions showed very good agreement with the analytical ones [15].

We have applied the DRBEM to investigate the effects of a temperature gradient at the exit of a cylindrical combustion chamber of length L and radius R [16]. It was assumed that the chamber walls were rigid, so that the normal velocity is zero v_n=0. At the open end of the chamber (exit), a radial velocity

$$v(r) = \exp\left(-\frac{r^2}{R^2} \right)$$

was considered and outside the chamber, a temperature distribution

$$T(x,r) = T_m \exp\left(-\mu \frac{Ar^2}{x_0 - x + L} \right)$$

was imposed at the interval $L<x<L+L_T$ (Fig. 17). A and x_0 are constants and $\mu = \ln(T_m / T_a)$, where T_m and T_a correspond to the maximum and ambient temperature.

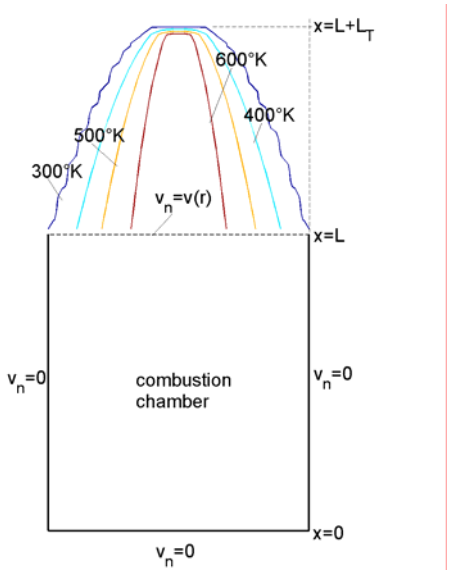

Figure 17: Combustion chamber with a hot region at the exit

Considering only a temperature gradient, the resulting inhomogeneous equation describing the wave propagation in the hot region is given by [17]:

$$\nabla^2 p + k_0^2 p = q$$
$$q = (k_0^2 - k^2)p - \frac{\nabla T}{T} \cdot \nabla p \qquad (18)$$

Expanding q as in Eq. (14) with:

$$f_j = 1 + r_j \quad ,$$
$$\psi_j = \frac{1 + r_j}{k_0^2} - \frac{2}{k_0^4} \frac{(1 - \cos(k_0 r_j))}{r_j^2} \qquad (19)$$

where $r_j = \left| \vec{x} - \vec{y}_j \right|$, and applying the boundary conditions of Eq. (12), the sound pressure at all points outside the combustion chamber could be calculated. The effects of the temperature gradient can be derived comparing the sound field with and without temperature gradient.

Calculations were made varying the maximum temperature T_m and the length of the hot region L_T [16]. As Fig. 18 shows, the sound power increases at low frequencies and reaches some approximately constant value at high frequencies. This value decreases uniformly with increasing T_m. This effect could be explained considering that more energy is reflected back into the hot region if the temperature is higher. In Fig. 19 can be seen, the higher the temperature the broader the radiation patterns become. This effect has to do with the refraction of the sound waves in the hot region due to the variable sound speed.

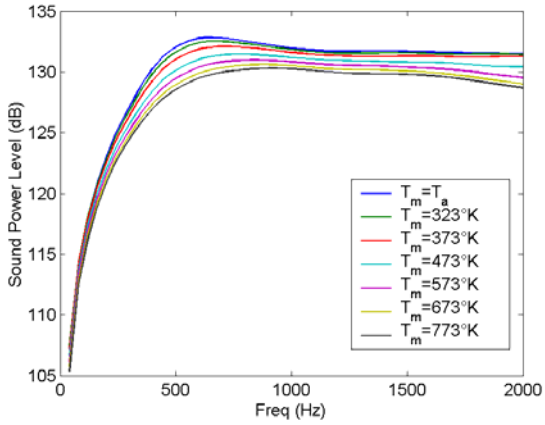

Figure 18: Dependence of the sound power with the maximum temperature

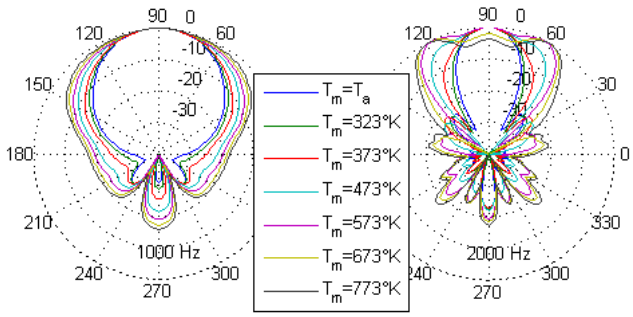

Figure 19: Dependence of the radiation patterns with the maximum temperature

7 SUMMARY

The present work yields a survey of numerical aspects of the coupling of a CFD method and an acoustic approach, here LES and BEM, for the determination of the radiated sound field by open and partly enclosed turbulent jet flames. Both methods are specialized techniques in their particular research field, the hybrid method provides the most effective way of calculating the fluid mechanical and combustion processes in the source region and the sound wave propagation in the ambient acoustic domain. But the coupling is complex process, including the choice of a coupling interface, data sampling at coarsened grids, Fourier Transform, inclusion of an infinite plane with an acoustic impedance and sound propagation in a non-homogeneous medium. The paper presents the actual state of research on these topics.

8 REFERENCES

[1] Ochmann M.: *Analytical und Numerical Methods in Acoustics*, in Mechel. F.P.: Formulas of Acoustics, 930-1026, Springer, (2002).

[2] Brick H., Piscoya R., Ochmann M., Költzsch P., *Modelling of combustion noise with the Boundary Element Method and Equivalent Source Method*, Proc. 33rd International Congress and Exposition on Noise Control – internoise 2004, Prague, (2004).

[3] Piscoya R., Brick H., Ochmann M., Költzsch P., *Numerical aspects of the Equivalent Source Method applied to combustion noise*, Proc. ICSV12, Lisbon, Portugal, (2005).

[4] Piscoya R., Brick H., Ochmann M., Költzsch P., *Application of equivalent sources to the determination of the sound radiation from flames*. Proceedings 13th International Congress on Sound and Vibration (ICSV13), Vienna, (2006).

[5] Brick H., Piscoya R., Ochmann M., Költzsch P., *Comparison of the Sound Radiation of Open Flames Simulated by a Hybrid Approach Using LES and ESM*, 11th CEAS-ASC Workshop on Experimental and Numerical Analysis and Prediction of Combustion Noise, Lisbon, Portugal (2007).

[6] Flemming F. et al., *A hybrid approach for the evaluation of the radiated noise from a turbulent non-premixed jet flame based on Large Eddy Simulation and equivalent source & boundary element methods*, Proc. ICSV12, Lisbon, Portugal, (2005).

[7] Jerry A. J, *The Shannon sampling theorem - Its various extensions and applications: A tutorial review*, Proc. IEEE 65, 1565-1596, (1977)

[8] Oppenheim A. V., Schafer R. W., Buck J. R., *Zeitdiskrete Signalverarbeitung*, Pearson Studium. München, (2004).

[9] Piscoya R., Brick H., Ochmann M., Költzsch P., *Equivalent Source Method and Boundary Element Method for calculating combustion noise,* Acta Acustica united with Acustica, accepted for publication, (2008).

[10] Bui P., Meinke M. and Schröder W.: *Numerical Applicability of Different Sound Source Formulations to Simulate Combustion Generated Noise Using a Hybrid LES/APE-RF Method*, 11th CEAS-ASC Workshop on Experimental and Numerical Analysis and Prediction of Combustion Noise, Lisbon, Portugal (2007).

[11] Ochmann M.: The complex equivalent source method for sound propagation over an impedance plane. Journal of the Acoustical Society of America 116, 3304-3311, (2004).

[12] Ochmann M., Brick H.: Acoustical Radiation and Scattering above an Impedance Plane. In: Marburg, S., Nolte, B. (Editoren): *Computational Acoustics of Noise Propagation in Fluids. Finite and Boundary Element Methods.* Chapter 17, 459{494, Springer-Verlag, Berlin, (2008).

[13] Welch P. D., *The use of the Fast Fourier Transform for the estimation of power spectra: A method based on time averaging over short, modified periodograms*, IEEE Transactions on Audio and Electroacoustics, 15(2), 70-73, (1967).

[14] Wrobel L. C.: *The boundary element method - Vol. 1: Applications in thermo-fluids and acoustics.* Wiley, (2002).

[15] Piscoya R., Ochmann M., *Sound propagation in a region of hot gas using the DRBEM*, Proceedings 14th International Congress on Sound and Vibration (ICSV14), Cairns, Australia (2007).

[16] Piscoya R., Ochmann M., *Einfluss von Temperaturgradienten auf den von Flammen abgestrahlten Schall*, Fortschritte der Akustik - DAGA 2008, Dresden, (2008)

[17] Perrey-Debain E., Gervais Y., Guilbaud M.: *Calcul de la propagation acoustique en milieux non homogènes infinis par la DRBEM*. C. R. Acad. Sci. Paris, t. 326, Séries II b, 649-659, (1998).